

DOI: 10.1070/QEL16023

Laser plume evolution in the process of nanopowder preparation using an ytterbium fibre laser

V.V. Osipov, G.S. Evtushenko, V.V. Lisenkov, V.V. Platonov, A.V. Podkin, E.V. Tikhonov, M.V. Trigub, K.V. Fedorov

Abstract. **We study the laser plume dynamics by means of high-speed shooting in the intrinsic light, as well as using the shadow method with a laser monitor. It is found that the laser plume arising under the impact of a radiation pulse from an ytterbium fibre laser with a power of 670 W on a Nd : Y_2O_3 target with an Nd concentration of 1 mol % is first a plasma consisting of the target material vapour, and then becomes a mixture of vapour and droplets. The first droplets in this plasma appear in ~200 μs after the formation of the laser plume, and in 400–500 μs the major part of the substance is removed in the form of liquid droplets. We have also found that the depth of the laser-produced crater linearly depends on the laser pulse duration, thus confirming the absence of essential shielding of laser radiation by melt droplets. The higher the target transparency, the longer the delay time of the formation of the laser plume and the greater its spread. Sometimes, instead of the laser plume formation, one can observe a light flash inside a semitransparent target. The explanation of these results is presented.**

Keywords: *laser plume, laser monitor, gas-phase method of nanoparticle preparation, ytterbium fibre laser.*

1. Introduction

The possibility of a high-efficiency production of oxide nanopowders by means of laser ablation using a cw CO_2 laser with an output power of 4 kW was first demonstrated in Ref. [1] and then developed in Ref. [2]. The method consists in the evaporation of a solid-state target having an appropriate composition by the radiation of a high-power laser with subsequent condensation of the vapour in a flow of a buffer gas (air). The potentiality of this approach was confirmed using a repetitively pulsed CO_2 laser with a mean output power of 600 W [3–5]. In the course of these studies, oxide nanopowders of various compositions [Y_2O_3 : ZrO_2(YSZ), Al_2O_3, Nd : Y_2O_3, CeGdO] were obtained. It was found that the powders synthesised using this method possess a number of unique advantages, such as the small mean size of nanoparticles, the narrow size distribution, the weak agglomeration of nanoparticles and the purity corresponding to that of the source material. Later, the dynamics and the spectrum of the intrinsic glow of the laser plume were studied, which allowed one to determine the plume temperature and composition [4–7], to clarify the effect of the composition and pressure of the buffer gas on the characteristics of nanopowders and the productivity of their preparation, as well as the energy efficiency of such approach [2, 3, 8]. As a result, the method was developed that allows the nanopowders, consisting of practically spherical particles, to be produced. In the process of evaporation of targets consisting of high-melting oxides by means of radiation from a repetitively pulsed CO_2 laser in an air flow at the atmospheric pressure, the arithmetical mean size of nanoparticles amounted to 10–15 nm. The size distribution function of nanoparticles has a strongly asymmetric shape and is close to the lognormal one, its width amounting to 35–40 nm. By varying the sort and pressure of the buffer gas, as well as the laser operation regime (continuous-wave or repetitively pulsed), it is possible to change the mean size of the produced particles within the interval 7–40 nm. The productivity of the nanopowder production depends on the thermal physical properties of the target material, the mean power of laser radiation, and can achieve 100 g h^{-1} [1]. The expenditures of the laser radiation energy in this case amount to ~7.5–24 W h g^{-1} [3].

The nanopowders based on Y_2O_3 and Al_2O_3 found applications in the synthesis of highly transparent ceramics, serving as active elements in solid-state lasers [9], while YSZ and CeGdO nanoparticles are used in solid electrolyte fuel elements [10].

High-power cw ytterbium fibre lasers have been recently used for the evaporation of targets [11–15]. The efficiency of these lasers is significantly higher than that of the CO_2 laser and achieves 25%–30%. However, the physical processes of interaction with the targets are essentially different for CO_2 and yttrium oxide fibre lasers, because in the process of nanoparticle production the target surface often becomes covered with a melted layer [12, 13, 15], which is transparent at the wavelength of the fibre laser radiation (1.07 μm) and nontransparent for the CO_2 laser (10.6 μm).

In this connection, the authors of Ref. [13] proposed a mechanism of the initial stage of laser irradiation of semitransparent targets. According to this mechanism, the radiation absorption occurs deep inside the target at the defects of the material crystalline structure, which are heated because of the absorption, the front region with respect to the laser beam

V.V. Osipov, V.V. Platonov, A.V. Podkin, E.V. Tikhonov Institute of Electrophysics, Ural Branch, Russian Academy of Sciences, ul. Amundsena 106, 620016 Ekaterinburg, Russia; e-mail: platonov@iep.uran.ru;
G.S. Evtushenko National Research Tomsk Polytechnic University, prosp. Lenina 30, 634050 Tomsk, Russia;
V.V. Lisenkov Institute of Electrophysics, Ural Branch, Russian Academy of Sciences, ul. Amundsena 106, 620016 Ekaterinburg, Russia; Ural Federal University named after the first President of Russia B.N. Yeltsin, ul. Mira 19, 620002 Ekaterinburg, Russia;
M.V. Trigub, K.V. Fedorov National Research Tomsk Polytechnic University, prosp. Lenina 30, 634050 Tomsk, Russia; V.E. Zuev Institute of Atmospheric Optics, Siberian Branch, Russian Academy of Sciences, pl. Akad. Zueva 1, 634055 Tomsk, Russia

Received 22 June 2016; revision received 1 August 2016
Kvantovaya Elektronika **46** (9) 821–828 (2016)
Translated by V.L. Derbov

being heated stronger. Due to the strong temperature dependence of the absorption coefficient, there arises a thermal wave that starts propagation from the defect to the target surface along the laser beam axis. Then, two scenarios are possible. If the temperature in the wave achieves the melting temperature with the appearance of a pressure jump, then the front surface of the target must break off. Otherwise, upon arrival of the wave at the target surface, its heating occurs until the material melting and evaporation, the split-off segments of the target surface having been observed in experiments [13]. Moreover, using indirect data Osipov et al. [15] supposed that a significant part of the material is removed from the target at the expense of splashing of liquid melt drops from the crater rather than the evaporation. The formation of a semitransparent fused layer and splashing of drops can be the causes of the formation of a rough relief on the target surface of Y_2O_3 activated with Nd ($Nd:Y_2O_3$) in the course of its evaporation and the reduction of the nanopowder productivity and mass yield by two times [14]. At the same time, when the target evaporation is implemented using a repetitively pulsed CO_2 laser, the nanopowder productivity is not reduced. As a result, for a similar mean radiation power (600 W) the productivity of the $Nd:Y_2O_3$ nanopowder preparation with a CO_2 laser appears by 1.4 times higher than that with a fibre laser [14].

However, for experimental substantiation of the above mechanism of the $Nd:Y_2O_3$ semitransparent target destruction by the radiation of a fibre laser it is necessary to detect the spread of large particles at the moment of the laser plume formation, or to detect the glow inside the target arising during the formation of a heat wave. From the technological point of view, it is important to know when there occurs a transition from the target evaporation mainly in the form of vapour to the droplet ablation. The correct choice of the pulse duration will allow a decrease in the content of large particles in the nanopowder, as well as an increase in the productivity and mass yield of the powder.

In this connection, the aim of the present work was to study the dynamics of the laser plume formed under the impact of the radiation pulse from the ytterbium fibre laser on the targets of $Nd:Y_2O_3$, YSZ and graphite by means of the high-speed frame-by-frame shooting in natural light emitted by the plume itself and using the laser monitor [16], as well as by photographing the glow inside the semitransparent target of $Nd:Y_2O_3$.

2. Experimental setup

The schematics of the experimental setups are presented in Fig. 1. To evaporate targets, we used an LS-07N ytterbium fibre laser (IRE-Polus, Fryazino) generating radiation at a wavelength $\lambda = 1.07$ μm in the cw regime with a power up to 700 W or in the repetitively pulsed regime with an instantaneous power up to 720 W. In our experiments, single rectangular pulses of this laser having a duration of 50–4000 μs were focused onto a target (*2*) by means of a silica lens (*1*). Its focal length F in most experiments was equal to 400 mm. In some experiments, we focused the radiation onto the target using a lens with $F = 200$ mm. The cases of using this lens will be specially mentioned below. The target was installed so that its surface was located in the middle of the laser beam waist. The laser spot on the target had the shape of a circle with a diameter of 250 or 430 μm, depending on the focal length of the lens. The distribution of the radiation intensity in the spot was close to Gaussian. To change the shape of the pulses we

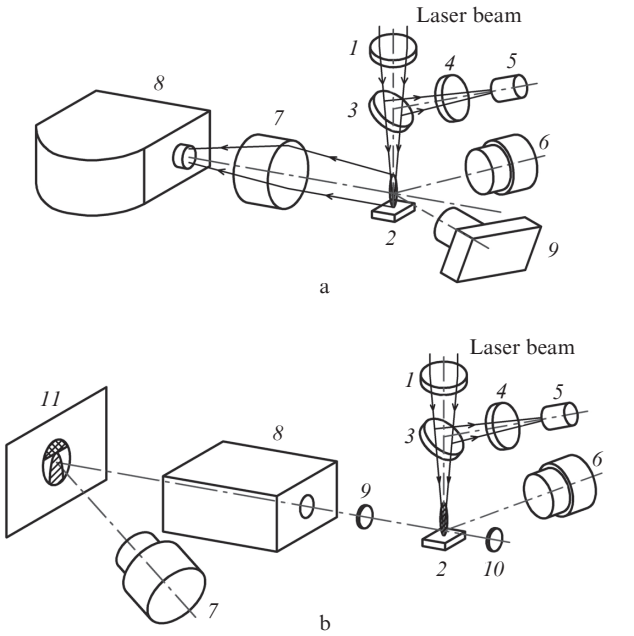

Figure 1. Schematics of the experimental setups for high-speed shooting of the laser plume spread in its intrinsic light (a) and using the laser monitor (b). The notations of the elements are presented in the text.

used a silica plate (*3*) that reflected a part of the beam through a filter (*4*) onto a SFN2500FA PIN photodiode (*5*). The instantaneous power of the radiation pulse at the laser output amounted to 720 W. With the partial reflection of radiation from the plate (*3*), the power of radiation at the target was 670 W, and the power density I averaged over the spot was equal to 1.4 MW cm^{-2} (for the lens with $F = 200$ mm) or 0.46 MW cm^{-2} (for the lens with $F = 400$ mm). After each radiation pulse the target was displaced. The laser plume glow in the visible light was recorded using a FEK-22 SPU-M photodetector (*6*). Its output signal and the signal from a PIN photodiode were measured using TDS520A and TDS5034B digital oscilloscopes. For the high-speed shooting of the plume in its intrinsic light we used a VFU-1 photographic setup [(*8*), Fig. 1a] with an additional objective [(*7*), Fig. 1a], which allowed recording 49 sequential images during one laser pulse. Depending on the pulse duration of the fibre laser, the interval between sequential frames amounted from ~5 to ~36 μs. For recording the images by means of the photographic setup, we used an ILFORD DELTA photographic film with a sensitivity of 400 ISO units in the spectral range 400–665 nm. Besides that, the laser plume was photographed using a CANON 350D photo camera [(*9*), Fig. 1a].

The high intensity of the intrinsic glow of the laser plume complicates a detailed study of splashing of large drops from the crater mouth. This could be done by means of an active optical system, a laser monitor, based on a CuBr laser (Fig. 1b), the operation of which is thoroughly described in Ref. [16]. In our experiments, it was used in the following way. A CuBr vapour active element [(*8*), Fig. 1b] simultaneously generated at two wavelengths (578.2 and 510.6 nm) the pulses of superradiation having a duration of 40 ns with a repetition rate of ~22 kHz. The mean power of superradiation was equal to 0.3 W. The radiation passed through the lens [(*9*), Fig. 1b] and was partially scattered by the laser plume. Then, the superradiation passed through the plume was partially reflected from a polished glass plate or a sheet of

white paper [(*10*), Fig. 1b], scattered again by the laser plume and passed again through the amplifying medium of the active element [(*8*), Fig. 1b]. From the other side of the active element, a screen [(*11*), Fig. 1b] was placed, on which a brightness-enhanced shadow image of the laser plume was formed by means of the lens [(*9*), Fig. 1b]. The screen image of the plume in its intrinsic light has very small brightness in comparison with the shadow image, since the width of the gain bands in the CuBr vapour active medium is very small (smaller than 0.005 nm). The image of the laser plume formed on the screen was recorded with a FastCam HiSpec 1 high-speed video camera [(*7*), Fig. 1b] with the time interval of 88 μs between the frames.

We studied $Nd:Y_2O_3$ targets of different density and degree of transparency. The first type of the target were tablets of pressed and sintered powder with the size of particles 1–10 μm. Its relative density ρ_{rel} (with respect to the density of Y_2O_3 single crystal) amounts to 57%. The absorption coefficient α of laser radiation with the wavelength λ = 1.07 μm by the present target amounts to 1.7×10^3 cm^{-1}, which corresponds to the penetration of radiation into the target to a depth of ~6 μm. Hence, such targets are conditionally referred to as 'nontransparent'. The other type of the target was ceramics samples sintered from a nanopowder with ρ_{rel} about 100%. The absorption coefficient of these samples varied within the limits α = 13–23 cm^{-1}, which corresponds to the radiation penetration depth 430–770 μm. These ceramic samples are conditionally referred to as 'semitransparent'. The methods of preparing the targets of both types are presented in Refs [14, 15].

We also studied nontransparent targets made of YSZ (with the Y_2O_3 concentration of 8.5 wt %) with $\rho_{rel} \approx 50\%$. In a number of experiments, the evaporated substance was pyrolitic graphite of MPG sort.

The depth and shape of the craters, formed in the targets under the impact of the fibre laser radiation, were measured by means of an Olympus BX51moptical microscope.

3. Experimental results and discussion

At the first stage, we studied the time behaviour of the laser plume integral glow. The data obtained using a FEK-22SPU-M photodetector are presented in Fig. 2. It is seen that the character of the plume glow variation in the case of evaporating nontransparent $Nd:Y_2O_3$ or YSZ targets appeared to be nearly similar (Figs 2a and 2b). In such cases, the intensity of the laser plume glow achieves a maximum in ~100 μs after the onset of the laser pulse. Then the observed plume brightness decreases, although the power of laser radiation does not change during the pulse. After the termination of the target irradiation, the oscillogram demonstrates a 'tail' of afterglow with a duration of more than 400 μs, caused by the emission from melt drops, as will be shown below.

In a semitransparent ceramic $Nd:Y_2O_3$ target the character of the glow oscillograms is almost the same. The differences consist in an increased delay of the plume glow appearance with respect to the laser pulse onset and a longer leading edge of the glow pulse. These effects can be easily explained, keeping in mind that laser radiation in such semitransparent targets is first absorbed by the structure defect, located inside the target at the depth of tens or hundreds of micrometres, which gives rise to a thermal wave [13]. To form a laser plume, this wave must reach the target surface. This is the explanation of the increased delay time of the laser plume formation

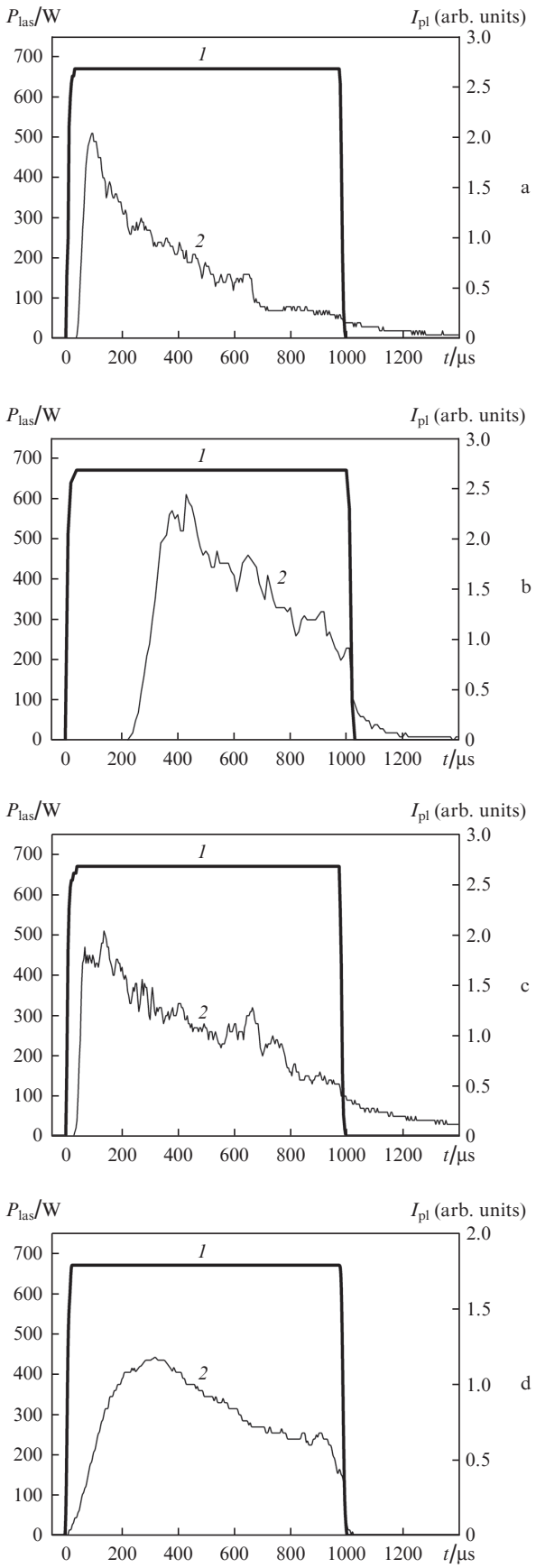

Figure 2. Oscillograms of (*1*) the fibre laser radiation pulse P_{las} and (*2*) the intensity of the laser plume glow I_{pl}, arising in the process of evaporating (a) nontransparent and (b) semitransparent ($\alpha \approx 21.8$ cm^{-1}) targets made of $Nd:Y_2O_3$, as well as (c) YSZ and (d) graphite targets.

as compared to the case of a nontransparent target, where the radiation of the fibre laser is absorbed in the near-surface layer with a thickness of ~6 μm.

Besides that, in all above oscillograms of the plume glow, one can observe intensity fluctuations, although the instantaneous power of the laser radiation remains unchanged. The most probable cause of this phenomenon is the transition from the ablation by evaporation to the vapour-droplet ablation, in which the shielding of radiation by the droplets leads to the variation of its intensity in the focal spot.

In the case of using a graphite target, no drops are expected to appear, since the graphite becomes evaporated by sublimation without the melt formation. Indeed, in this case the following specific features are seen in the oscillogram (Fig. 2d). The delay time of the plume appearance is minimal, the glow of the plume stops practically at the moment of the laser pulse termination, and the glow intensity increases during a longer time. Finally, the most important feature is that the oscillogram is sufficiently smooth and has no expressed spikes. Some distortions are probably caused by a small signal-to-noise ratio due to much lower brightness of the laser plume from the graphite target as compared to the oxide targets.

The most difficult for explanation is the observed reduction of the laser plume brightness in 100–300 μs after the plume formation, observed in all targets (Fig. 2). It may be due to a temperature decrease in the mouth of the laser-produced crater and, therefore, due to a decrease in the entire laser plume temperature. A decrease in the glow intensity may be also caused by an increase in the crater depth in the process of the laser pulse action and by shielding a part of radiation by splashed drops. To clarify the situation, we studied the dependence of the crater depth on the duration of the laser radiation pulse, keeping its peak power unchanged. These studies allowed the determination of the crater depth and the pulse duration, at which the radiation cannot reach the crater bottom, being scattered and absorbed by the drops. The data for the $Nd:Y_2O_3$ targets with different transparency are presented in Fig. 3. To account for the statistical spread, we have measured and averaged the depths of 5–10 craters, formed under similar irradiation conditions. In order to increase the reliability, the studies were performed with the targets of different transparency, as well as with different radiation power densities, which was implemented using lenses with a different focal length.

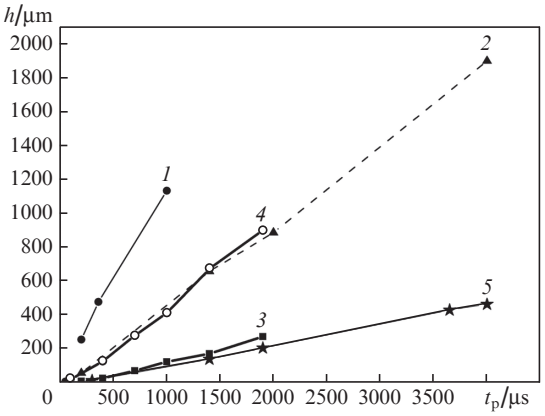

Figure 3. Dependences of the mean depth h of the craters, formed in (*1*, *2*) nontransparent and (*3*, *4*; $\alpha = 21.8$ cm^{-1}) semitransparent $Nd:Y_2O_3$ targets and (*5*) graphite on the duration of the laser radiation pulses. The instantaneous power of the pulses on the target is 670 W, the focal length of the lens is [(*1*, *4*); $I = 1.4$ MW cm^{-2}] 200 and [(*2*, *3*, *5*); $I = 0.46$ MW cm^{-2}] 400 mm.

The comparison of the obtained results shows that the crater in a nontransparent target appears to be nearly three times deeper than in a semitransparent one. For example, for the pulse duration 1.9 ms and the lens with $F = 400$ mm, the crater depth in a nontransparent target attains ~900 μm, while in a semitransparent target with the absorption coefficient $\alpha = 21.8$ cm^{-1} it is only 280 μm. Such a significant difference is explained by several reasons. First, the relative density of the nontransparent target is by two times smaller than that of the semitransparent one, i.e., the removal of the same amount of the material leads to crater depth values differing by two times. Second, in the semitransparent target the laser radiation first penetrates into the target to a greater depth, which requires more energy before the target begins to evaporate. It is easy to see that, independent of the target transparency, under the focusing of radiation into the spot with the diameter 250 μm ($I = 1.4$ MW cm^{-2}) the craters produced on the target surface are, on the average, by 3–4 times deeper than in the case of a larger spot diameter (430 μm) and smaller radiation power density ($I = 0.46$ MW cm^{-2}).

The obtained data clearly show that, independent of the radiation intensity and the target density, the dependence of the crater depth on the pulse duration is linear. No bends of the plot are observed that could indicate any acceleration of the material release from the target due to a change in the ablation mechanism. This observation means that the melt temperature in the crater is not decreased during the pulse action, and the droplets splashed from the crater do not inhibit the supply of the laser radiation energy to the target. Therefore, one of the main reasons of a decreasing intensity of the laser plume glow is a decrease in the power density of laser radiation at the inclined walls of the crater with its deepening, which leads to a decrease in the evaporated substance flow. This hypothesis is confirmed by the fact that in the case of graphite evaporation in ~400 μs after the plume formation the decrease in its glow brightness is also observed. In this case, the craters with the depth to 460 μm (the pulse duration 4 ms, $I = 0.46$ MW cm^{-2}) are also produced, and the dependence of the crater depth on the laser pulse duration is linear. Thus, based only on the analysis of the dynamics of the laser plume glow brightness and the depth of the craters produced in the $Nd:Y_2O_3$ target we were unable to determine unambiguously the moment of time, when the removal of the substance due to splashing of droplets begins to dominate over the evaporation. This was one more reason for studying the laser plume dynamics using a high-speed shooting technique.

Figure 4 presents negative images of laser plumes arising in the process of the laser pulse action on the targets made of different materials. The images were obtained by means of the VFU-1 setup. For convenience, in these images the time is indicated relative to the moment of the laser plume appearance. In particular, Fig. 4a shows the photographs of the laser plume for the case of the nontransparent $Nd:Y_2O_3$ target. This case is implemented, when in the process of the nanopowder production the target is not yet covered with a melted layer. Here the target destruction begins in 36 μs after the onset of the laser pulse, during which the radiation melts the target substance and brings it to boiling (for Y_2O_3 the boiling temperature is $T_{boil} = 4300$ °C [17]). After the beginning of evaporation, a glowing column of vapour appears above the target surface, the height of which first increases and in 178 μs after

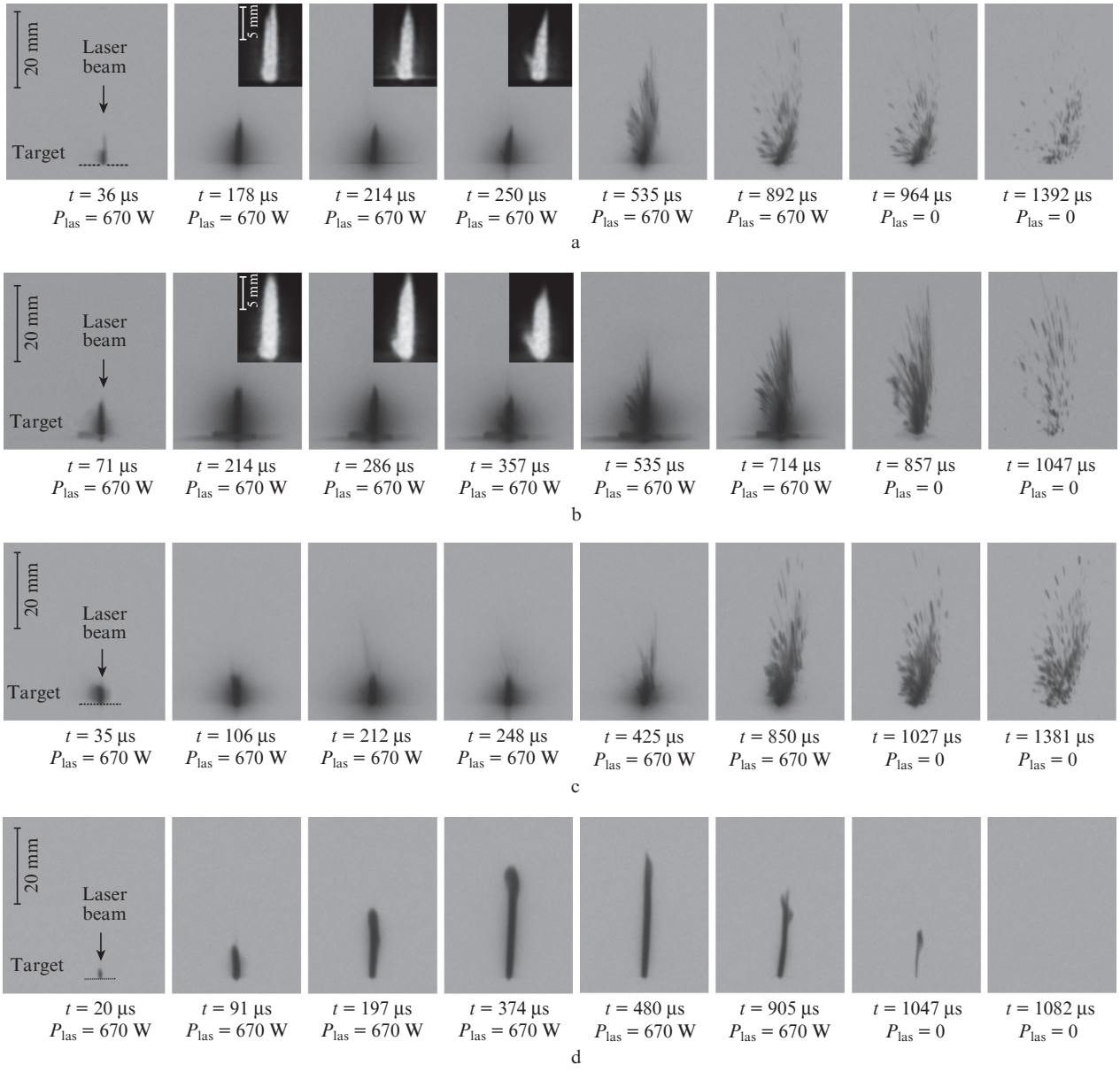

Figure 4. Photographs in the light of the laser plume, produced in the process of evaporating (a) nontransparent and (b) semitransparent (α = 21.8 cm^{-1}) $Nd:Y_2O_3$ targets and (c) YSZ and (d) graphite targets by the radiation pulse having the duration 1.0 ms. The time is indicated relative to the moment of the plume appearance. The delay of the plume appearance with respect to the onset of the laser pulse is t_{del} = (a) 38, (b) 285, (c) 28 and (d) 8 μs; P_{las} is the instantaneous power of the fibre laser radiation.

the laser plume appearance reaches a maximal value of ~12 mm. During the next 72 μs, in spite of the unchanged instantaneous power of laser radiation, the height of the column slightly decreases to 10 mm. During the first ~200 μs after the formation of the laser plume its shape (the column) and dynamics are in qualitative agreement with those observed in Refs [4, 7], where the YSZ and Nd:YAG targets were evaporated in air by means of a radiation pulse from a CO_2 laser having a duration of 330 μs and an intensity I = 1–1.3 MW cm^{-2}. In these papers it was found that the glow of the column is caused by the light emission by the vapour of YO, ZrO, AlO and NdO radicals at a temperature of ~4300 °C near the target surface. The nanoparticles are produced due to the condensation of this vapour. One should expect that in our experiments the laser plume glow at this stage is caused by the glow of YO and NdO radicals. However, in ~200 μs after the beginning of the target evaporation by the radiation of the fibre laser the plume begins to develop in a way different from the case of CO_2 laser. A number of tracks caused by the spread of large-scale objects appear at the photographs of the laser plume. Earlier analysis of the contents of the evaporation chamber in the course of nanopowder synthesis [13] has shown that such objects are mostly droplets of the melt. In the same paper, the size distribution function of the droplets is presented. In ~500 μs after the beginning of target evaporation the laser plume consists predominantly of the droplets, and the fraction of the glowing vapours is essentially reduced.

It is interesting to clarify, when the first large-scale objects begin to fly out of the produced crater, but the high brightness of the vapour column glow in the photographs of the plume (Fig. 4) makes it impossible. Therefore, a few photographs were subjected to additional digital processing and are presented in Fig. 4a as magnified images in the insets. In the photograph corresponding to the time moment t = 214 μs one

can easily see a track of some large-scale object that flew out of the crater and is located not far from the crater mouth. However, at the previous photograph, corresponding to the time moment $t = 178$ μs, it is still absent. As mentioned above, these large-scale objects are probably drops of the liquid melt having the size of a few tens (to a hundred) of micrometres [13], which are splashed from the crater by the vapour pressure. With time, the number of droplets outgoing from the crater only grows. In the photographs taken after the moment of time $t = 535$ μs one can see that the most part of the substance begins to be removed from the crater by splashing of the droplets rather than by their evaporation. After the termination of the laser pulse, the glowing droplets are still seen in the photographs during ~400 μs, which explains the long-time afterglow of the plume in the oscillogram (Fig. 2a). The spread of numerous liquid droplets occurs also under the action of the fibre laser radiation pulse on the semitransparent $Nd:Y_2O_3$ target with the absorption coefficient $\alpha = 21.8$ cm^{-1} at the wavelength 1.07 μm (Fig. 4b) and the YSZ target (Fig. 4c). In the process of evaporating semitransparent yttrium oxide, the tracks of the first spreading droplets are clearly seen at the crater mouth in the photograph exposed at the moment of time $t = 286$ μs. The droplets are also formed in the case of focusing the laser radiation by the lens with $F =$ 200 mm onto the YSZ targets, semitransparent and transparent $Nd:Y_2O_3$ targets, and a piece of the nontransparent $Nd:Y_2O_3$ target, covered by a semitransparent melted layer.

For the graphite target evaporated under the same conditions no spread of large-scale particles was observed (Fig. 4d). In this case, the laser plume consists only of the vapour column that reaches its maximal height of 32 mm in 480 μs after its appearance. The absence of spreading droplets, in our opinion, is due to the fact that under the atmospheric pressure and the temperature 4200 °C the graphite is sublimated without forming a liquid melt [17]. This confirms our idea that the large-scale particles observed in the evaporation of $Nd:Y_2O_3$ and YSZ targets are drops of a liquid melt splashed from the crater by the vapour pressure.

Moreover, the obtained experimental results apparently demonstrate the absence of large fragments that could be split from the target surface at the moment of the laser plume formation and then spread in the air. Note also, that the absence of bends in the linear dependence of the crater depth on the duration of laser radiation pulse is due to the early transition from the vapour to the vapour-droplet ablation and the small amount of material extracted in the vapour form.

The establishment of the moment, when the large-scale particles and liquid droplets appear, is the principal result of the present paper. However, because of a too bright glow of the vapour of radicals, the tracks of colder and less bright droplets in the photographs made in the intrinsic light of the plume are observed only beyond the vapour column or after it vanishes. Under these conditions, it is impossible to determine the moment of the first drops production precisely and, even more, to detect the separation and spread of the target fragments at the moment of the laser plume formation.

Unambiguous determination of the spread of solid-state particles is possible at the initial stage by suppressing the strong backlight of the vapour glow and photographing their shadows by means of a monochromatic intense radiation from another laser. This technique was implemented using the laser monitor [16] for high-speed video recording of the laser plume. Figure 5a shows the photographs of the plume formed by the evaporation of the semitransparent $Nd:Y_2O_3$ target with the absorption coefficient $\alpha \approx 30.7$ cm^{-1}. They are shadow images of the laser plume free of its own glow. In the photographs, one

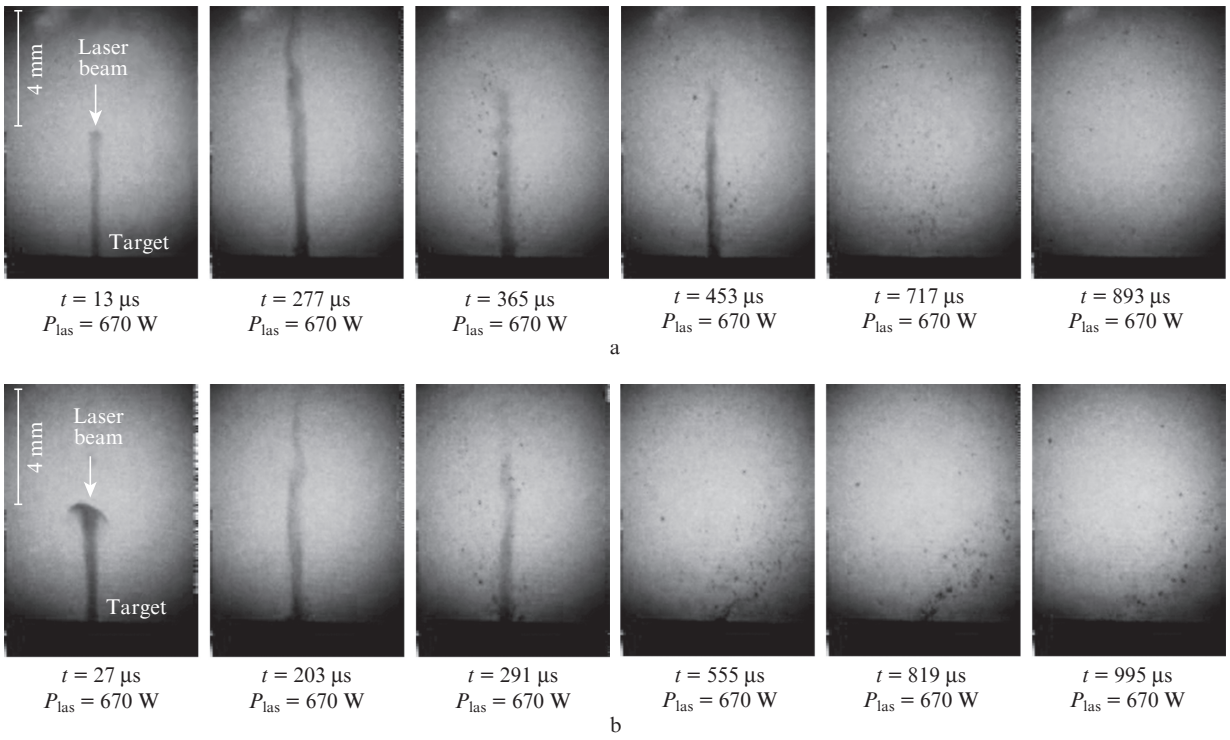

Figure 5. Photographs of the laser plume obtained using the laser monitor in the case of evaporating (a) semitransparent ($\alpha \approx 30.7$ cm^{-1}) and (b) nontransparent $Nd:Y_2O_3$ targets by the radiation pulse with the duration 1400 μs (the time t is indicated relative to the moment of the plume appearance, P_{las} is the instantaneous power of the fibre laser radiation).

can see well that, first, in the zone illuminated by the CuBr laser radiation beam an extended vapour column appears. Its height increases, and in 277 μs after the column appearance its top edge moves beyond the laser monitor field of view (9.5×6.7 mm). At this moment at the mouth of the crater, one can see the first large droplet pushed out from the crater by the vapour pressure. Then, although the power of the fibre laser radiation remains constant, the image of the column begins to reduce in size and vanishes completely at the time moment t = 717 μs. Simultaneously the number of spreading droplets grows. We calculated the initial velocity for some of them. For different droplets it appeared to be 12–60 m s^{-1}. Given the initial velocity of the very first outgoing droplet (23 m s^{-1}), we can estimate that it has left the crater in ~200 μs after the appearance of the laser plume. An analogous situation was observed in the evaporation of the nontransparent $Nd:Y_2O_3$ target under the same conditions (Fig. 5b). The estimates show that the splashing of the first droplets begins in 150 μs, i.e., somewhat earlier than for the semitransparent target. This is explained by a smaller relative density of the nontransparent target and, therefore, a faster crater formation. The data on the beginning of the first large-scale droplets spread obtained in this experiment agree well with the results of high-speed photography of the laser plume in its intrinsic light.

The photographs of the ablation of the semitransparent $Nd:Y_2O_3$ target by the radiation of the fibre laser directly show that at the moment of the laser plume formation the large particles having the size of tens and hundreds of micrometres are not produced and are not spread in the air. This fact gives rise to doubts concerning the validity of the thermal wave mechanism [13] that seems to provide a convincing explanation of the unusual target destruction. However, the strong dependence of the laser plume appearance delay time t_{del} on the absorption coefficient of the target material and its huge statistical spread can be well explained only by this mechanism. Indeed, for α = cm^{-1} the range obtained by us is Δt_{del} = 20–1000 μs, and for α = 1700 cm^{-1} we have Δt_{del} = 11–57 μs, which, according to this mechanisms, is due to the different depth of the defects location.

In order to confirm the existence of the above mechanism, we visualised the thermal wave in the semitransparent $Nd:Y_2O_3$ target. For this purpose, the edge of the ceramic sample having the thickness of 2 mm was polished. We managed to detect the thermal wave by shooting the process of the laser action on the semitransparent $Nd:Y_2O_3$ target with a photo camera (Fig. 6). The glow is seen to start at the depth of 1.0–1.2 mm, and the glowing channel spreads to the surface of the target.

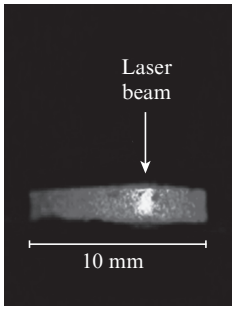

Figure 6. Photograph of the thermal wave glow in the semitransparent $Nd:Y_2O_3$ target (α = 21.6 cm^{-1}).

Obviously, the energy of radiation introduced into the target is sufficient to form the light flash inside the propagating thermal wave, but is insufficient for bringing the material to the melting temperature and, therefore, for the mechanical destruction of the front surface of the target. The absence of the laser plume in this photograph means that the laser pulse in this case has terminated before the beginning of the target surface melting. The split-off fragments observed in the mouth of some craters are, obviously, due to other mechanisms, probably by the significant temperature gradient near the crater. Their explanation requires additional research.

4. Conclusions

By studying the dynamics of the laser plume arising under the impact of the radiation pulse of the ytterbium fibre laser having a power of 670 W and a duration 50–4000 μs, focused on semitransparent ($Nd:Y_2O_3$) and nontransparent ($Nd:Y_2O_3$ or YSZ with the Y_2O_3 concentration of 8.5 weight percent) targets, we have established the following facts. At the initial stage the laser plume is a column of the target material vapour, and in ~200 μs the droplets of melt begin to be splashed from the produced crater, the droplet size exceeding 10 μm. Their number grows with time, and in the next ~500 μs the laser plume appears to consist mainly of droplets. It is shown that the dependence of the crater depth on the laser radiation power has a linear character, thus indicating the absence of essential shielding of the laser radiation by the melt droplets. Thus, at the pulse duration exceeding 500–700 μs the major fraction of the material is removed from the target by splashing of the melt droplets, and the vapour fraction appears to be small. Naturally, for an essential increase in the vapour fraction it is necessary to stop the action of the laser radiation on the target before the moment, at which the splashing of large-scale drops from the crater begins. This condition will be fulfilled for the laser pulse durations below 200 μm.

In the semitransparent $Nd:Y_2O_3$ target with the Nd concentration of 1 mol % the glowing channel was found, the appearance of which is related to the thermal wave, propagating along the laser beam from the defect of the crystal structure, initially absorbing the radiation, to the surface of the target. The energy of laser radiation, introduced into the channel, is sufficient for exciting the glow, but insufficient of melting the target material in the channel. This explains the absence of a pressure jump in the channel and, as a consequence, the absence of mechanical destruction of the target surface and the large-scale particles in the photographs, made at the moment of the plume formation.

Acknowledgements. This work was partially supported by the Russian Foundation for Basic Research (Grant Nos 13-08-00529-a and 14-08-00181-a), and also within the frameworks of the State Task No. 0389-2014-0027. The development of the laser monitor for plume imaging was supported by the Russian Science Foundation (Grant No. 14-19-00175).

References

1. Müller E., Oestreich Ch., Popp U., Michel G., Staupendahl G., Henneberg K.-H. *KONA Powder and Particle J.*, **13**, 79 (1995).
2. Kurland H.-D., Grabow J., Muller F.A. *J. Eur. Ceram. Soc.*, **31**, 2559 (2011).
3. Osipov V.V., Kotov Yu.A., Ivanov M.G., Samatov O.M., Lisenkov V.V., Platonov V.V., Murzakayev A.M., Medvedev A.I., Azarkevich E.I. *Laser Phys.*, **16** (1), 116 (2006).

4. Osipov V.V., Solomonov V.I., Platonov V.V., Snigireva O.A., Lisenkov V.V., Ivanov M.G. *Laser Phys.*, **16** (1), 134 (2006).
5. Osipov V.V., Solomonov V.I., Platonov V.V., Snigireva O.A., Ivanov M.G., Lisenkov V.V. *Kvantovaya Elektron.*, **35**, 467 (2005) [*Quantum Electron.*, **35**, 467 (2005)].
6. Osipov V.V., Solomonov V.I., Platonov V.V., Snigireva O.A., Ivanov M.G., Lisenkov V.V. *Kvantovaya Elektron.*, **35**, 633 (2005) [*Quantum Electron.*, **35**, 633 (2005)].
7. Osipov V.V., Platonov V.V., Lisenkov V.V. *Kvantovaya Elektron.*, **39**, 541 (2009) [*Quantum Electron.*, **39**, 541 (2009)].
8. Osipov V.V., Platonov V.V., Lisenkov V.V., in *Handbook of Nanoparticles* (Switzerland: Springer International Publishing, 2015) Vol. 2. DOI 10.1007/978-3-319-13188-7_8-1.
9. Bagaev S.N., Osipov V.V., Ivanov M.G., Solomonov V.I., Platonov V.V., Orlov A.N., Rasuleva A.V., Vatnik S.M. *Opt. Mater.*, **31**, 740 (2009).
10. Ivanov V.V., Lipilin A.S., Kotov Yu.A., Khrustov V.R., Shkerin S.N., Paranin S.N., Spirin A.V., Kaygorodov A.S. *J. Power Sources*, **159**, 605 (2006).
11. Ivanov M.G., Kopylov Yu.L., Kravchenko V.B., Zayats S. *Phys. Status Solidi C*, **10** (6), 940 (2013).
12. Osipov V.V., Platonov V.V., Lisenkov V.V., Podkin A.V., Zakharova E.E. *Phys. Status Solidi C*, **10** (6), 926 (2013).
13. Lisenkov V.V., Osipov V.V., Platonov V.V. *Zh. Tekh. Fiz.*, **83** (10), 78 (2013) [*Tech. Phys., Rus. J. Appl. Phys.*, **58** (10), 1469 (2013)].
14. Osipov V.V., Lisenkov V.V., Platonov V.V., Orlov A.N., Podkin A.V., Savvin I.A. *Zh. Tekh. Fiz*., **84** (5), 97 (2014) [*Tech. Phys., Rus. J. Appl. Phys*., **59** (5), 724 (2014)].
15. Osipov V.V., Lisenkov V.V., Platonov V.V., Orlov A.N., Podkin A.V., Savvin I.A. *Zh. Tekh. Fiz.*, **84** (5), 88 (2014) [*Tech. Phys., Rus. J. Appl. Phys*., **59** (5), 716 (2014)].
16. Evtushenko G.S., Trigub M.V., Gubarev F.A., Evtushenko T.G., Torgaev S.N., Shiyanov D.V. *Rev. Sci. Instrum.*, **85** (3), 033111 (2014).
17. Grigor'ev I.S., Meilikhov E.Z. (Eds) *Handbook of Physical Quantities* (Boca Raton, FL: CRC Press, 1997; Moscow: Energoatomizdat, 1991).